

Available online at www.sciencedirect.com

SCIENCE @ DIRECT®

Chemical Physics xxx (2003) xxx–xxx

Chemical
Physicswww.elsevier.com/locate/chemphys

On the energy dependence of the Zeeman and hyperfine parameters in the $\tilde{A}^2\Sigma^+$ state of OH and OD

Ju Xin^a, Ionela Ionescu^b, David Kuffel^b, Scott A. Reid^{b,*}^a Department of Physics and Engineering Technologies, Bloomsburg University, Bloomsburg, PA 17815, USA^b Department of Chemistry, Marquette University, P.O. Box 1881, Milwaukee, WI 53201-1881, USA

Received 13 March 2003; in final form 13 March 2003

8 Abstract

9 We report quantum beat studies of the energy dependence of the Zeeman parameters in the $\tilde{A}^2\Sigma^+$ state of OH and
10 OD, and the nuclear hyperfine parameters of OD($\tilde{A}^2\Sigma^+$). In contrast to previous work, we find that the sign and
11 magnitude of the anisotropic g -factor g_1 for $v' = 0$ is consistent with that expected from Curl's relationship. However, at
12 higher energies g_1 changes sign, a result we attribute to interaction with the repulsive $1^4\Pi$ state, which is known to lead
13 to predissociation at higher energies. The magnetic and electric quadrupole hyperfine constants were determined for
14 OD($\tilde{A}^2\Sigma^+$, $v' = 0-3$), and the constants for $v' = 2, 3$ are reported here for the first time. The derived values are consistent
15 with previous experimental results and available ab initio calculations.

16 © 2003 Published by Elsevier Science B.V.

18 1. Introduction

19 The hydroxyl radical is an important species
20 in atmospheric and combustion chemistry and
21 astrophysics [1,2], and the subject of numerous
22 experimental [3–56] and theoretical [57–74] inves-
23 tations. Much of this work has focused on the
24 ultraviolet $\tilde{A}^2\Sigma^+ \leftarrow \tilde{X}^2\Pi$ system, which was ob-
25 served in flames and electric discharges more than
26 80 years ago [2]. The $\tilde{A}^2\Sigma^+$ state correlates with
27 O(1D) + H(2S) products, and is crossed by several
28 repulsive states ($^2\Sigma^-$, $^4\Sigma^-$, $^4\Pi$) correlating with

O(3P) + H(2S), [41] providing a classic example of
Case I predissociation [2]. Experimental studies
[41,46,50,52,55] show that for low N the onset of
predissociation occurs at $v' = 2$ for OH and $v' = 3$
for OD, and the trends in lifetime as a function of
excited rotational and vibrational state are well
reproduced by ab initio calculations [67,73,74]. At
higher energies, theoretical studies [68–72] predict
that interferences among direct and indirect path-
ways will lead to asymmetric (Fano) lineshapes and
a pronounced wavelength dependence of the
product yields, which has been observed experi-
mentally in only a few cases [75–80]. Thus, experi-
mental and theoretical interest in this molecule
continues to this day.

Spectroscopic studies of the $\tilde{A}^2\Sigma^+ \leftarrow \tilde{X}^2\Pi$ sys-
tem have examined the rotational and fine structure

* Corresponding author. Tel.: +414-288-7565; fax: +414-288-7066.

E-mail address: scott.reid@mu.edu (S.A. Reid).

[9,27], hyperfine structure [25,26,33,39,40,42,44, 54], and Zeeman [22,25,26,33,38,40,42,53,54] and Stark [23,26] effects. Metcalf and co-workers [15,22] used the Hanle effect, level crossing spectroscopy, and optical double resonance to determine Landé g -factors for some rotational levels in $\tilde{A}^2\Sigma^+(v' = 0)$. Zare and co-workers [16,25,26] employed zero- and high-field level crossing and optical-radio frequency double resonance to determine the OD hyperfine constants, radiative lifetime and Landé g -factors in $\tilde{A}^2\Sigma^+(v' = 0)$, and conducted Stark measurements to determine the excited state dipole moment [26]. Subsequently, Metcalf and co-workers [38,40,42] applied the quantum beat technique to measure Landé g -factors for OH $\tilde{A}^2\Sigma^+(v' = 0)$, and the same method was used by Carter et al. [54] to probe the $\tilde{A}^2\Sigma^+(v' = 0)$ level of OD and the OD·Ar van der Waals complex. The ensuing years have witnessed increasingly precise measurements of the hyperfine parameters for the $v' = 0, 1$ levels in the $\tilde{A}^2\Sigma^+$ state of OH and OD [39,44,54], which are in reasonable agreement with available ab initio predictions [59].

In light of these studies, it is surprising that fundamental questions remain regarding the Zeeman parameters of the $\tilde{A}^2\Sigma^+$ state. For example, Coxon conducted a two-state fit of the measured spectrum for the $\tilde{A}^2\Sigma^+ \leftarrow \tilde{X}^2\Pi$ system of OD [30], and found that the spin–rotation splittings in the $\tilde{A}^2\Sigma^+$ state of OD arose predominantly from a second order spin–orbit interaction with $\tilde{X}^2\Pi$ (a case of “pure precession”). Therefore, Curl’s relationship [81] for the anisotropic correction to the electron spin g -factor, g_1 , should approximately hold. However, a recent quantum beat study [54] of OD($\tilde{A}^2\Sigma^+, v' = 0$) determined a value of the correct sign but an order of magnitude larger than expected from Curl’s relationship. In addition, the reported electron spin g -factor was significantly larger than the free electron value. These results were attributed to mixing with excited quartet states [54]. We find this surprising, in that the $\tilde{A}^2\Sigma^+(v' = 0)$ level of OD lies ~ 4000 cm^{-1} below the opening of the lowest dissociation channel, and $\sim 24\,000$ cm^{-1} below the lowest lying quartet state ($^4\Sigma^-$) in the Franck–Condon region [67]. Moreover, such an effect should also be found for OH($\tilde{A}^2\Sigma^+, v' = 0$), which is not the case [42]. Thus,

there is a need for further studies of the Zeeman effect in the $\tilde{A}^2\Sigma^+$ state and its energy dependence.

Our group has been interested for several years in the application of high-resolution quantum beat methods to free radicals [82–85]. The quantum beat method offers the advantages of other coherent time-domain spectroscopies [86], with an intrinsic resolution (~ 160 kHz for a radiative lifetime of 1 μs) capable of revealing molecular hyperfine structure and splittings induced by weak magnetic or electric fields. As a prelude to the application of quantum beat methods to polyatomic radicals, and in view of the unanswered questions regarding the Zeeman parameters in the $\tilde{A}^2\Sigma^+$ state, we undertook a detailed study of the energy dependence of the Zeeman parameters for both OH and OD, and also report the magnetic and electric quadrupole hyperfine constants for OD ($v' = 0-3$).

2. Experimental procedure 112

2.1. Experimental apparatus 113

The apparatus consisted of a cubic, black-anodized vacuum chamber evacuated by a 6 in. diffusion pump (Varian VHS-6) and equipped with a molecular beam source and fluorescence detection assembly. The chamber was surrounded by a tri-axial Helmholtz coil system (Walker Scientific) used to null the earth field and generate fields for Zeeman experiments. Power to each coil came from independent power supplies (Kepco), and the field strength was calibrated using a Hall effect Gaussmeter. The field vector was oriented along the detection (space fixed X) axis, perpendicular both to the direction of laser propagation (along the space fixed Y axis) and to the polarization axis of the linearly polarized laser beam (oriented along the space fixed Z axis). In this configuration the selection rule for Zeeman quantum beats is: $\Delta M_F = \pm 2$.

The laser system consisted of a tunable, frequency doubled, etalon narrowed dye laser (Lambda-Physik Scanmate 2E) pumped by the second (532 nm) or third (355 nm) harmonic of a Nd:YAG laser (Continuum Powerlite 7010). The following dyes or dye combinations were used: R640/R610 (OH and OD, $v' = 0$), R6G (OH and

138 OD, $v' = 1$), C540 (OD, $v' = 2$), C307 (OD, $v' = 3$;
139 OH, $v' = 2$). The laser output passed through a
140 linear polarizer (CVI laser, $10^5:1$ extinction) prior
141 to entering the chamber. Typical pulse energies
142 were 10–200 μJ , and the unfocused beam was of
143 ~ 3 mm diameter. The pulse energy was increased
144 with increasing v' to offset the decreasing Franck–
145 Condon factor.

146 The OH (OD) radicals were generated by a
147 pulsed electrical discharge through a mixture of
148 H_2O (D_2O) in Argon, generated by passing Ar at a
149 typical backing pressure of 20 psig through a
150 bubbler containing H_2O (D_2O) at room tempera-
151 ture. The mixture was expanded into vacuum via a
152 commercial pulsed valve (General Valve IOTA-1),
153 modified by the addition of a ring electrode dis-
154 charge assembly [87]. The discharge was initiated
155 by a negative going 800 V pulse of ~ 20 μs dura-
156 tion, which passed through a 10 k Ω ballast resis-
157 tor, and was set near the falling edge of the gas
158 pulse to minimize the effects of the transient
159 magnetic field generated by the (magnetically ac-
160 tivated) valve. The timing of laser, nozzle, and
161 discharge firing was controlled via a digital delay
162 generator (Stanford Research Systems DG535),
163 which generated the gate pulse for the high voltage
164 pulser (Directed Energy GRX-1.5K-E). The laser
165 beam crossed the molecular beam at a distance of
166 ~ 15 mm (30 nozzle diameters) downstream. Flu-
167 orescence was collected at right angles to both the
168 laser and molecular beam by a two lens $f/2.4$
169 condenser assembly, and passed through a UV
170 polarizer (Meadowlark Optics) prior to striking a
171 photomultiplier tube detector (Orion) held at
172 typically -550 V. The PMT output was terminated
173 into 50 Ω and digitized by an oscilloscope (HP
174 54521A) operated at a sampling rate of 1 GHz and
175 record length of 4096 points.

176 Under typical experimental conditions, the OH
177 (OD) radicals were produced almost exclusively in
178 the $J = 3/2$ level of the $^2\Pi_{3/2}$ state, and we esti-
179 mate a rotational temperature of ≈ 10 K from a
180 comparison of intensity ratios for $\text{R}_{21}(2)/\text{R}_{21}(1)$
181 and $\text{R}_{11}(2)/\text{R}_{11}(1)$ pairs. Zeeman quantum beats
182 were observed on the $\text{S}_{21}(1)$, $\text{R}_{21}(1)$, $\text{R}_{11}(1)$, and
183 $\text{Q}_{11}(1)$ transitions, which provided access to ex-
184 cited state levels with $N = 1-3$ and $J = 3/2-5/2$.
185 Transition frequencies were obtained from [9,27].

2.2. Data collection and analysis procedures

186

187 Pairs of waveforms were collected at a given
188 magnetic field strength for parallel and perpen-
189 dicular orientations of the detector polarization
190 with respect to the polarization axis of the laser,
191 achieved by rotating a linear ultraviolet (UV) po-
192 larizer (Meadowlark Optics) placed between the
193 condenser lens system and PMT. The waveforms
194 were typically averaged over 2500 laser shots. The
195 time-dependent degree of polarization $[P(t)]$ was
196 calculated for each pair according to the equation:

$$P(t) = \frac{I_{\parallel}(t) - I_{\perp}(t)}{I_{\parallel}(t) + I_{\perp}(t)}. \quad (1)$$

198 Fig. 1 displays representative data for the $\text{R}_{21}(1)$
199 transition in the $v' = 1 \leftarrow v'' = 0$ band of OH at a
200 field strength of 2.72 G. The upper panel displays
201 the waveforms, and the lower panel the calculated
202 degree of polarization. Consistent with the theory
203 of anisotropic quantum beats, the modulations in

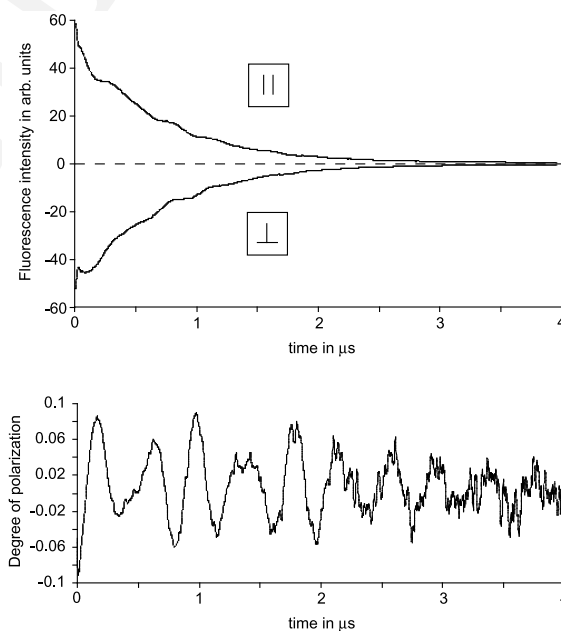


Fig. 1. Upper panel: Waveforms observed following excitation of the $\text{R}_{21}(1)$ transition in the $v' = 1 \leftarrow v'' = 0$ band of OH at a magnetic field strength of 2.72 G, obtained in parallel (top) and perpendicular (bottom) orientations of laser and detection polarizations. Lower panel: Degree of polarization calculated following Eq. (1) in the text.

4

J. Xin et al. / Chemical Physics xxx (2003) xxx–xxx

204 the two waveforms exhibit a phase shift of 180° ,
205 and reduced amplitude for the perpendicular
206 configuration.

207 The Fourier transform of $P(t)$ was obtained
208 using PSIplot software. Fig. 2 displays the trans-
209 form of the $P(t)$ shown in Fig. 3, which reveals two
210 strong quantum beats. The center frequencies were
211 obtained by fitting each peak to a Gaussian function
212 using the Marquardt–Levenburg method. We
213 tested both Gaussian and Lorentzian functions,
214 and obtained similar goodness-of-fit statistics for
215 isolated peaks. The fits to a Gaussian function
216 typically gave correlation coefficients ≥ 0.999 ,
217 with a typical standard deviation of 30 kHz in the
218 determined peak center frequency. This procedure
219 was repeated for 8–10 different field strengths in
220 the range over which linear tuning was observed.
221 For OH, this range extended to the highest fields
222 used (~ 10 G), while for OD to fields below ~ 5 G,
223 consistent with the observations of Zare and co-
224 workers [16,25,26]. Beats arising from different
225 hyperfine components (inter-manifold beats) were
226 not observed for OH, as the hyperfine splittings
227 are much larger than the coherence width of our
228 laser [44]. Thus, the Lande' factor for a given F
229 component was determined by a linear fit of the

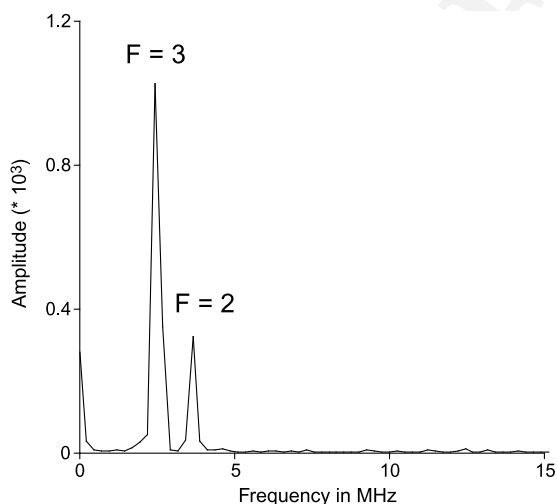


Fig. 2. Fourier transform of the degree of polarization data shown in bottom panel of Fig. 1. The beats are labeled in terms of the excited state hyperfine quantum number.

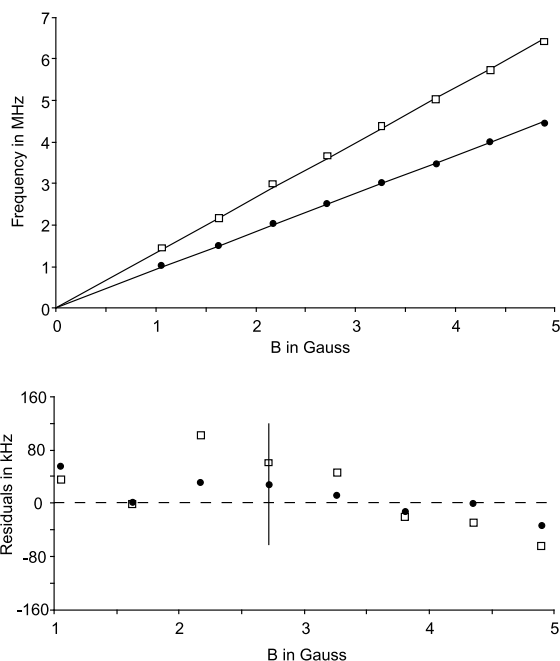


Fig. 3. Upper panel: Magnetic field dependence of the quantum beat frequencies for the $R_{21}(1)$ transition in the $v' = 1 \leftarrow v'' = 0$ band of OH. The lines mark linear fits to the data. Lower panel: Fit residuals.

magnetic field dependence of the intra-manifold 230
beat frequency using the formula: 231

$$\omega = 2\mu_B B g_F, \quad (2)$$

where $\mu_B = 1.39967 \text{ MHz G}^{-1}$. An example for the 233
 $R_{21}(1)$ transition of the $v' = 1 \leftarrow v'' = 0$ band of 234
OH is shown in Fig. 3, which includes the residuals 235
to the linear fit and a typical error bar describing 236
the uncertainty in our determination of the peak 237
position. 238

For OD, hyperfine (zero-field) quantum beats 239
were also observed, as initially reported by Huber 240
and co-workers [53,54]. Fig. 4 displays a typical OD 241
quantum beat spectrum, obtained for the $R_{21}(1)$ 242
transition of the $v' = 1 \leftarrow v'' = 0$ band at a field 243
strength of 2.72 G. A global least squares fit was 244
performed to determine the Lande' factors for each 245
 F component and the zero-field hyperfine splittings, 246
from which the hyperfine coupling constants were 247
determined as described below. The inter-manifold 248
beat frequencies were fit using the formula: 249

$$\omega = \Delta + \mu_B B [M_F g_F - M_{F'} g_{F'}], \quad (3)$$

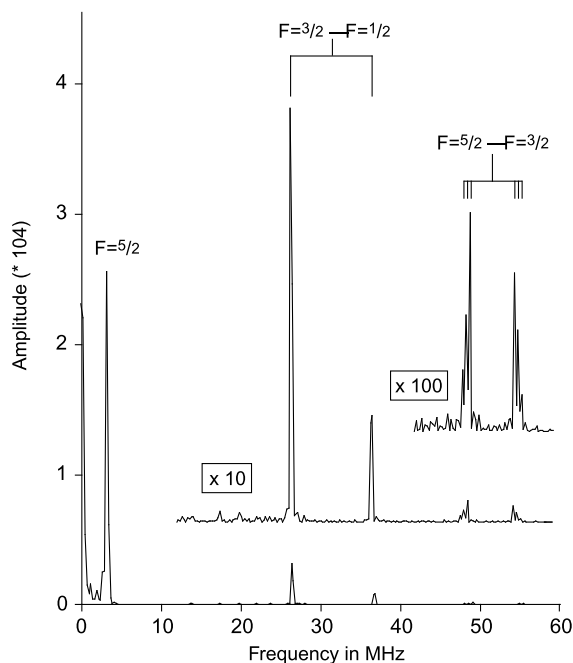


Fig. 4. Zeeman quantum beat spectrum of the $R_{21}(1)$ transition in the $v' = 1 \leftarrow v'' = 0$ band of OD at a field strength of 2.72 G. The intra- and inter-manifold beats are labeled in terms of the excited state hyperfine quantum numbers.

251 where Δ is the zero-field splitting of the two com-
 252 ponents F, F' . This procedure was followed for all
 253 transitions except $R_{11}(1)$, where the inter-manifold
 254 beats were particularly weak and difficult to ob-
 255 serve above the noise. In this case, the zero-field
 256 splittings were obtained from a zero-field spectrum
 257 averaged over 5000 laser shots, and the Lande'
 258 factors were determined from the intra-manifold
 259 beats, following Eq. (2).

260 3. Theory and data modeling procedures

261 The $A^2\Sigma^+$ state of OH conforms to case $b_{\beta J}$
 262 coupling [16,25,26], where $\mathbf{J} = \mathbf{N} + \mathbf{S}$ and $\mathbf{F} =$
 263 $\mathbf{J} + \mathbf{I}$, and $\mathbf{I} = \mathbf{I}_{H(D)}$. Consistent with previous
 264 treatments [22,25,26,33,38,40,42,53,54], for Zee-
 265 man experiments involving an unperturbed state
 266 with rotational angular momentum N the follow-
 267 ing Hamiltonian was assumed:

$$H = H_{sr} + H_{hfs} + H_Z, \quad (4)$$

where 269

$$H_{sr} = \gamma \mathbf{N} \cdot \mathbf{S} \quad (5)$$

is the spin-rotation interaction [25,26]. For OH 271
 the hyperfine Hamiltonian [88]: 272

$$H_{hfs} = b \mathbf{I} \cdot \mathbf{S} + c I_z S_z \quad (6)$$

was used, where b, c are the Frosch and Foley 274
 constants and the Fermi-contact interaction is gi- 275
 ven by $b + c/3$. For OD, the Hamiltonian included 276
 a quadrupolar coupling term: [33,88] 277

$$H_{hfs} = b \mathbf{I} \cdot \mathbf{S} + c I_z S_z + eqQ \left[3I_z^2 - \frac{I(I+1)}{4I(2I-1)} \right]. \quad (7)$$

The effective Zeeman Hamiltonian for a dia- 279
 tomic molecule in a $^2\Sigma^+$ state can be expressed as: 280
 [89,90] 281

$$H_Z = g_s \mu_B B_0 T_{p=0}^1(\mathbf{S}) + g_1 \mu_B B_0 \sum_{q=\pm 1} D_{0q}^{(1)}(\omega) T_q^1(\mathbf{S}) \\ - g_r \mu_B B_0 T_{p=0}^1(\mathbf{N}) - g_N \mu_N B_0 T_{p=0}^1(\mathbf{I}), \quad (8)$$

where the first term is the isotropic electron spin 283
 interaction, the second term represents anisotropic 284
 corrections to g_s , the third term accounts for the 285
 rotational Zeeman effect, and the final term rep- 286
 represents the nuclear Zeeman effect. We included 287
 the nuclear Zeeman term in our analysis for both OH 288
 and OD. 289

The Hamiltonian matrix elements were evalu- 290
 ated in the case $b_{\beta J}$ basis. The hyperfine matrix 291
 elements were taken from Radford [88], using the 292
 correction noted by German [33], while the Zee- 293
 man matrix elements were taken from [90]. The 294
 Hamiltonian matrix was factored into submatrices 295
 for $J = N \pm 1/2$ and $F = J \pm 1/2$ (for $I = 1/2$) or 296
 $F = J + I, J + I - 1, \dots, J - I$ (for $I = 1$). The 297
 matrix was of size 4×4 for OH, and for OD either 298
 5×5 or 6×6 . We used published spin-rotation 299
 constants for OD($v = 0-3$) [30], and determined 300
 the hyperfine coupling constants b, c , and eQq by 301
 fitting the zero-field hyperfine splittings to values 302
 calculated by diagonalizing each submatrix with 303
 $B_0 = 0$. The diagonalization used a Jacobian 304
 transformation, and the fitting a least-squares 305
 routine. For OH, we used the hyperfine and spin- 306
 rotation constants for $v' = 0$ and 1 determined by 307
 ter Meulen et al. [44] and the parameters for $v' = 2$ 308

were estimated from the energy dependence of the OD parameters. The rotational dependence of γ was neglected in our analysis, at it varies by only $\sim 0.2\%$ over the range $N = 1-3$ [44].

We first diagonalized each submatrix at a single value of the field strength (B_0) in the range employed. Changing the value of B_0 in this range did not alter the calculated values, consistent with our observation of linear Zeeman tuning. The calculated Zeeman energies were averaged over all pairs of Zeeman sublevels of a given hyperfine component differing in M_F by 2, and divided by $\mu_B B_0$ to give the theoretical g_F factor. The calculated g_F factors were fit to the experimental values using a least-squares algorithm. In practice, we found that the data set did not allow simultaneous determination of the three g -factors: g_s , g_1 , and g_r , a fact also noted by Carter et al. [54] in QBS studies of OD($\tilde{A}^2\Sigma^+$, $v = 0$). In that work, the value of g_r was constrained to be zero, since the predicted magnitude (~ 0.002) is around three times smaller than the value of g_1 predicted from Curl's relationship. However, the matrix elements for this term are typically 4–5 times larger than those for g_1 , and the relative contributions of these terms may thus be similar. We fixed g_s at the free electron value (2.002), and used g_1 , and g_r as fit parameters, a procedure similar to that used by Raab et al. [42] in QBS studies of OH($\tilde{A}^2\Sigma^+$, $v' = 0$).

It is well known that fitted g -factors are sensitive to uncertainties in rotational constants and

fine structure parameters [25,26,91]. For OD, the uncertainty in γ varies from $\sim 0.1\%$ for $v' = 0$ to $\sim 9\%$ for $v' = 3$ [30]. We conducted a series of fits of the data for OD($v' = 3$) to assess the sensitivity of the fitted values to uncertainties in γ and the hyperfine constants b , c , and eQq . Only the former produced a noticeable change, with the 9% uncertainty in γ leading to a 30% change in the fit value of g_1 and 11% change in the fit value of g_r . These are significantly smaller than the experimental uncertainties.

4. Results and discussion

4.1. Zeeman parameters

Tables 1 and 2 list the experimental low field g_F -factors determined for various hyperfine levels in the $v' = 0, 1$, and 2 levels of OH($\tilde{A}^2\Sigma^+$) and the $v' = 0, 1, 2$, and 3 levels of OD($\tilde{A}^2\Sigma^+$). For OH($v' = 0$) (Table 1) the previous (and more precise) results of [42] are included for comparison. Due to the short lifetime of OH($v' = 2$), it was not possible to obtain data for the weak $S_{21}(1)$ transition, however, the data obtained for other rotational levels in this band is similar in precision to those for $v' = 0$ and 1, which demonstrates that QBS can be applied to the study of predissociating states.

Tables 3 and 4 list the fit values of g_1 and g_r for OH($v' = 0-2$) and OD($v' = 0-3$), respectively. In a

Table 1
Experimental g_F -factors for the $\tilde{A}^2\Sigma^+$ state of OH

N	J	F	Experimental g_F factors			
			$v' = 0^a$	$v' = 0^b$	$v' = 1^b$	$v' = 2^b$
3	2.5	3	-0.2412(2)	-0.2397(9)	-0.2417(8)	^c
		2	-0.3336(6)	-0.3338(26)	-0.3387(17)	^c
2	2.5	3	0.3308(2)	0.3282(20)	0.3290(12)	0.3265(12)
		2	0.4701(6)	0.4747(30)	0.4754(22)	0.4743(33)
2	1.5	2	-0.3078(3)	-0.3087(17)	-0.3070(7)	-0.3103(34)
		1	-0.4991(6)	-0.5015(37)	-0.5011(24)	-0.5144(27)
1	1.5	2	0.4973(8)	0.4969(29)	0.5002(37)	0.4962(48)
		1	0.8649(14)	0.8633(49)	0.8807(90)	0.8819(75)

^a Ref. [42].

^b This work.

^c Not determined.

Table 2
Experimental g_F -factors for the $A^2\Sigma^+$ state of OD

N	J	F	Experimental g_F factors			
			$v' = 0$	$v' = 1$	$v' = 2$	$v' = 3$
3	2.5	3.5	-0.2022(16)	-0.2020(10)	-0.2036(18)	-0.2052(28)
		2.5	-0.2582(23)	-0.2631(25)	-0.2594(20)	-0.2662(34)
		1.5	-0.4061(28)	-0.4020(30)	-0.4097(35)	-0.4176(55)
2	2.5	3.5	0.2786(11)	0.2799(15)	0.2841(21)	0.2815(18)
		2.5	0.3603(20)	0.3600(34)	0.3663(29)	0.3658(39)
		1.5	0.5659(40)	0.5681(35)	0.5735(43)	0.5696(41)
2	1.5	2.5	-0.2434(14)	-0.2407(10)	-0.2459(12)	-0.2459(17)
		1.5	-0.2994(29)	-0.2996(49)	-0.2936(96)	-0.303(11)
		0.5	-0.666(18)	-0.665(16)	-0.685(30)	-0.675(34)
1	1.5	2.5	0.3982(17)	0.3988(19)	0.4059(30)	0.4015(24)
		1.5	0.5020(94)	0.5064(64)	0.510(17)	0.510(11)
		0.5	1.141(30)	1.141(24)	1.140(55)	1.139(36)

Table 3
Zeeman parameters for the $A^2\Sigma^+$ state of OH

v'	g_s^a	g_1	g_r	σ^b
0	2.002	-0.020(10)	0.0035(22)	0.0035
1	2.002	-0.002(8)	0.0013(18)	0.0028
2	2.002	0.007(13)	0.0056(33)	0.0041

^a Fixed.^b Standard deviation of the fit.Table 4
Zeeman parameters for the $A^2\Sigma^+$ state of OD

v'	g_s^a	g_1	g_r	σ^b
0	2.002	-0.001(8)	0.001(2)	0.0041
1	2.002	0.000(8)	0.000(2)	0.0040
2	2.002	0.016(11)	0.002(2)	0.0053
3	2.002	0.010(10)	0.004(2)	0.0049

^a Fixed.^b Standard deviation of the fit.

367 two-state model, g_1 can be predicted from the
368 perturbation treatment of Curl [81]

$$g_1 \cong -\frac{\gamma}{2B}. \quad (9)$$

370 Using the reported constants [9,27,44], the calcu-
371 lated value for ($\tilde{A}^2\Sigma^+$, $v' = 0$) is ~ -0.007 . Our
372 experimental results for OH $\{g_1 = -0.020(4)\}$ and
373 OD $\{g_1 = -0.001(8)\}$ bracket this value. To in-
374 crease the precision, we conducted a global fit of
375 the OH and OD values, using the appropriate
376 dependence on reduced mass for g_r . The value

derived from this fit, $g_1 = -0.007(7)$ (Table 5), is in
good agreement with that calculated from Eq. (9).

Our fit value of g_1 for OD ($v' = 0$) is much
smaller than that of Carter et al. [54] who report
 $g_1 = -0.095(41)$. This discrepancy does not arise
from the analysis procedure, as when fitting our
results with g_r set to 0.0 we derive g_1 and g_s values
of 0.004(36) and 1.997(35), respectively. Although
Carter et al. [54] did not include the nuclear Zee-
man effect in their analysis, we find that the mag-
nitude of this effect for OD is at the precision of
our measurements, and thus cannot account for
the discrepancy. We have also not identified any
systematic error (field calibration, etc.) that could
reasonably explain this result, and thus at present
the origin of this discrepancy remains unexplained.

If g_1 was determined solely via coupling with
 $\tilde{X}^2\Pi$, its value should not depend on v' , since the
second-order contribution that gives rise to γ is
proportional to \tilde{B} . Indeed, the observed decrease in
 γ with increasing v' in OD ($\tilde{A}^2\Sigma^+$), from 0.12010(12)
 cm^{-1} for $v' = 0$ to 0.106(9) cm^{-1} for $v' = 3$, closely

Table 5
Zeeman parameter values for the combined fits

v' (OH/OD)	g_s^a	g_1	g_r	σ^b
0/0	2.002	-0.007(7)	0.0028(25)	0.0045
2/3	2.002	0.011(9)	0.0056(38)	0.0055

^a Fixed.^b Standard deviation of the fit.

399 mirrors the decrease in \tilde{B} , from 9.04351(12) cm⁻¹
400 for $v' = 0$ to 8.0746(5) for $v' = 3$ [30]. Our results, in
401 contrast, show that with increasing v' , g_1 changes
402 sign (Tables 3 and 4), although the effect is near the
403 limit of our experimental precision. The upper panel
404 of Fig. 5 displays a combined plot of the vi-
405 brational energy dependence of g_1 for OH and OD
406 in the $\tilde{A}^2\Sigma^+$ state. To better resolve this trend, as
407 noted above we conducted a simultaneous fit of the
408 g -factors for OH and OD levels lying close in energy
409 $\{v' = 0$ (OH) with $v' = 0$ (OD), and $v' = 2$ (OH)
410 with $v' = 3$ (OD)}, and the derived parameters are
411 listed in Table 5.

412 Turning to the rotational g -factor (g_r), the val-
413 ues determined for OH($v' = 0$) and from a simul-
414 taneous fit of the $v' = 0$ data for OH and OD are
415 consistent with the (more precise) value of
416 0.00248(6) determined by Raab et al. [42] and with
417 calculations based on coupling to $\tilde{X}^2\Pi$ [42]. The
418 lower panel of Fig. 5 shows the vibrational energy

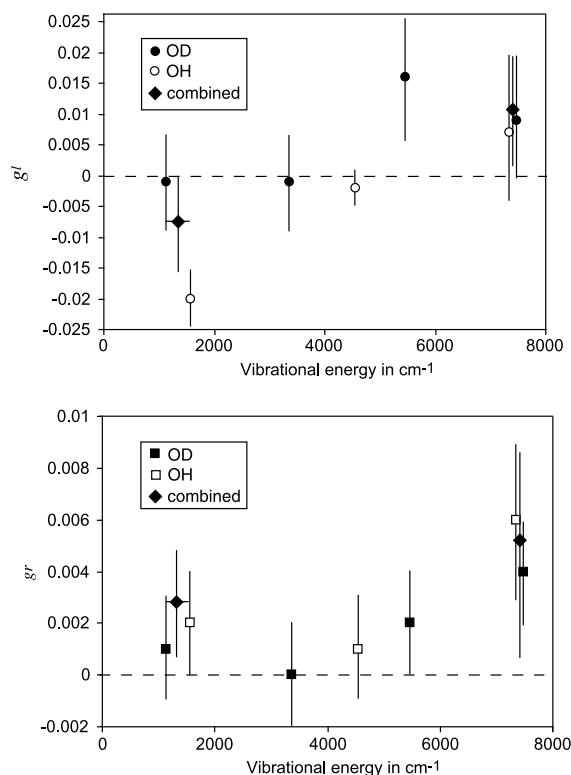


Fig. 5. Upper panel: Fit values of g_1 for OH, OD, and the combined fits plotted against vibrational energy in the $\tilde{A}^2\Sigma^+$ state. Lower panel: Similar plot for g_r .

dependence of g_r for OH and OD in the $\tilde{A}^2\Sigma^+$ 419
state. It appears that g_r increases at higher energies 420
(Tables 3–5), but the trend is not outside our ex- 421
perimental uncertainty. 422

We considered several explanations for the ob- 423
served energy dependence of g_1 , which are sum- 424
marized below. 425

4.1.1. Interactions with higher lying Π states 426

A change in sign of g_1 could arise from inter- 427
actions with higher lying Π states, leading to a 428
change in sign of the energy denominator in the 429
second-order contribution: [89–92] 430

$$g_1^e \cong \sum_{\Pi} \frac{\langle \Pi | AL^+ | \Sigma \rangle \langle \Sigma | L^+ | \Pi \rangle}{E_{\Sigma} - E_{\Pi}}. \quad (10)$$

Candidates include $2^2\Pi$, which correlates to 432
 $O(^1D) + H(^2S)$ and is calculated to lie $\sim 48,000$ 433
cm⁻¹ above $\tilde{A}^2\Sigma^+$ [61], and the repulsive $1^4\Pi$ state, 434
which correlates to $O(^3P) + H(^2S)$ and lies slightly 435
higher than $2^2\Pi$ in the Franck–Condon region 436
[61,67]. The $1^4\Pi$ state should be more important, 437
as the configuration of this state differs from that 438
of $\tilde{A}^2\Sigma^+$ by one spin–orbital [93]. Using the ab 439
initio potential curves and spin–orbit matrix ele- 440
ment at $R = 2.0$ bohr [67,73], from which a value 441
for $\langle \Pi | AL^+ | \Sigma \rangle$ of ~ 200 cm⁻¹ is derived [93], we 442
estimate a contribution to g_1 from the $\tilde{A}^2\Sigma^+ - 1^4\Pi$ 443
interaction of ~ 0.007 for the highest v' . 444

4.1.2. Interactions with higher lying Σ state(s) 445

Interactions with the higher lying $1^4\Sigma^-$ state can 446
influence g_1 via the third-order term: [92] 447

$$g_1^{e(3)} \cong - \sum_{4\Sigma} \frac{\langle 2\Sigma | H_{SO} | 4\Sigma \rangle^2}{[E_{2\Sigma} - E_{4\Sigma}]^2}. \quad (11)$$

However, as the sign of this term is negative, it 449
would lead to a decrease in g_1 . Moreover, given the 450
calculated spin–orbit matrix element (H_{SO}) be- 451
tween $\tilde{A}^2\Sigma^+$ and $1^4\Sigma^-$ in the Franck–Condon re- 452
gion (-2.2 cm⁻¹ at $R = 2.00$ bohr) [67,73], 453
the contribution from this term is negligibly small. 454

4.1.3. Modification of g_s via interactions with higher lying states 455

In our analysis, we fixed g_s at the free electron 457
value. This might not be a good assumption, as 458

Table 6
Experimental hyperfine level splittings (in MHz) for the $A^2\Sigma^+$ state of OD

N	J	F'	F''	Experimental hyperfine level splittings in MHz				
				$v' = 0^a$	$v' = 0^b$	$v' = 1$	$v' = 2$	$v' = 3$
3	2.5	3.5	2.5	52.90	52.84(3)	53.50(4)	54.37(4)	55.44(4)
		2.5	1.5	37.86	37.91(2)	38.49(3)	38.94(3)	39.72(4)
2	2.5	3.5	2.5	78.55	78.58(2)	79.25(3)	80.02(4)	81.13(4)
		2.5	1.5	57.18	57.31(3)	57.72(2)	58.34(4)	59.17(4)
2	1.5	2.5	1.5	51.40	51.35(2)	52.02(2)	52.85(2)	54.04(3)
		1.5	0.5	31.03	31.10(3)	31.57(2)	32.10(2)	32.76(2)
1	1.5	2.5	1.5	94.37	94.29(3)	95.04(3)	96.00(4)	97.32(4)
		1.5	0.5	58.50	58.71(2)	59.16(3)	59.76(4)	60.56(3)

Not determined.

^a Ref. [54].

^b This work.

459 interactions with $2^2\Pi$ and $1^4\Pi$ can modify g_s via
460 the third order term [92,94]:

$$g_s^{(3)} \cong - \sum_{\Pi} \frac{|\langle \Pi | H_{so} | \Sigma \rangle|^2}{[E_{\Sigma} - E_{\Pi}]^2}. \quad (12)$$

462 However, as the sign of this term is negative, ne-
463 glecting it should produce a *decrease* in the fit
464 value of g_1 . Moreover, based upon the ab initio
465 matrix elements [67,73], these terms are negligibly
466 small in the Franck–Condon region.

467 On the basis of these considerations, we sug-
468 gest that the energy dependence of g_1 may reflect
469 the $\tilde{A}^2\Sigma^+ - 1^4\Pi$ interaction, which is known to
470 lead to predissociation at higher energies. The
471 estimated contribution to g_1 is of the correct sign
472 and order of magnitude; however, it is curious
473 that this effect should not be manifest in the $\tilde{A}^2\Sigma^+$
474 spin–rotation constants [30], and at present we
475 have no explanation for this. Further analysis
476 would benefit from additional calculations, par-
477 ticularly of the radial dependence of the L^+
478 matrix element, and additional experiments en-
479 compassing a larger range of N , which would al-
480 low a more precise determination of the energy
481 dependence of g_r [42].

482 4.2. Hyperfine parameters

483 Table 6 lists the experimental hyperfine splittings
484 determined in this work for OD($\tilde{A}^2\Sigma^+$, $v' = 0-3$),

and compared with the results of Carter et al. [54] 485
for $v' = 0$. Table 7 compares the determined hy- 486
perfine parameters (b , c , eQq and the Fermi-contact 487
constant $b + c/3$) with previous measurements and 488
theoretical predictions for $v' = 0$ and 1. Our results 489
are generally in good agreement with the QBS 490
measurements of Carter et al. [54] and previous 491
experimental studies [25,26,33]. 492

The Fermi-contact hyperfine constant ($b + c/3$) 493
is proportional to the spin density of the unpaired 494
electron, $|\psi(0)|^2$, at the deuterium nucleus. As the 495
O–D bond is stretched, this term should approach 496
the value for the 2S state of atomic deuterium, 497
which is 218.256 MHz [95]. Thus, an increase in 498

Table 7
Hyperfine parameters (in MHz) for the $A^2\Sigma^+$ state of OD

v'	b	c	$b + c/3$	eqQ
0^a	110.182(20)	24.72(11)	118.42	0.238(30)
0^b	109.73(5)	25.73(20)	118.31(14)	0.22(5)
0^c	110.18(3)	24.85(17)	118.46(7)	0.29(5)
0^d	112.7	25.4	121.2	0.262
1^b	111.15(5)	24.40(20)	119.28(14)	0.05(4)
1^c	111.29(5)	23.81(24)	119.23(10)	0.20(10)
1^d	115.7	24.3	123.8	0.258
2^c	112.63(8)	22.78(40)	120.22(14)	0.30(13)
3^c	114.49(8)	21.40(39)	121.62(15)	0.31(13)

^a Experiment [54].

^b Experiment [33].

^c Experiment, this work.

^d Theory [59].

499 this term with increasing v' is expected, and clearly
500 observed (Table 7). The calculations [59] repro-
501 duce this trend but overestimate its magnitude,
502 predicting a $\sim 2\%$ increase in going from $v' = 0-1$,
503 while the experiment shows an increase of only
504 $\sim 0.7\%$. Ter Meulen et al. [44] observed a similar
505 trend for OH, with $b + c/3$ increasing by $\sim 0.2\%$ in
506 going from $v' = 0-1$.

507 The parameter c represents the dipole–dipole
508 interaction, given by: [88]

$$c = 3g_e g_1 \mu_B \mu_N \left\langle \frac{P_2(\cos \theta)}{r^3} \right\rangle, \quad (13)$$

510 where g_e and g_1 are the electron and nuclear g -
511 factors, μ_B and μ_N are the Bohr and nuclear
512 magneton, the argument of the Legendre polynomial
513 $P_2(x) = (3x^2 - 1)/2$ is the cosine of the angle
514 of the electron coordinate with respect to the in-
515 ternuclear axis, and r is the distance between the
516 electron and the nucleus of spin I. For OH, ter
517 Meulen et al. [44] observed a significant ($\sim 10\%$)
518 decrease in c in going from $v' = 0-1$. We find a
519 decrease of $\sim 4\%$ for OD, in reasonable agreement
520 with the results of German [33] and theoretical
521 predictions [59]. This trend continues to higher
522 energy, with a total decrease of $\sim 14\%$ in going
523 from $v' = 0-3$.

524 The magnitude of c is usually interpreted in
525 terms of a p orbital on the nucleus in question;
526 however, for protons the p orbital lies too high in
527 energy to contribute, and the dominant contribu-
528 tion comes from interaction of the deuterium nu-
529 cleus with the oxygen atom unpaired spin-density
530 [96]. Indeed, the ground state c constants in a se-
531 ries of XH radicals approximately scale with the
532 inverse cube of the equilibrium internuclear separa-
533 tion (r_e) [96]. As a simple test of this hypothesis,
534 we plot in Fig. 6 the experimental values for c
535 versus the inverse cube of the average value of the
536 internuclear separation r approximated from the
537 data of Coxon [30]. The graph is linear to within
538 our experimental precision, and a fit using linear
539 regression is shown as the solid line in Fig. 6.

540 In contrast to b and c , the small quadrupolar
541 coupling constant eQq is not well determined, and
542 no obvious dependence on energy is found to
543 within our experimental precision. Our findings
544 are consistent with theoretical predictions [59], and

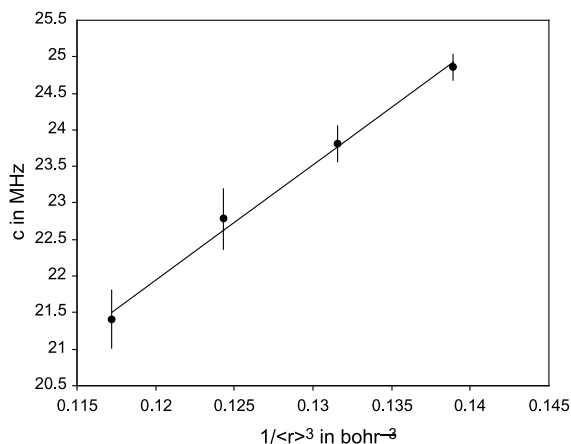


Fig. 6. Fit values for the dipole–dipole hyperfine constant c of OD($\tilde{A}^2\Sigma^+$, $v' = 0-3$) plotted against the inverse cube of the average internuclear separation approximated from the data of [30]. The solid line marks a linear fit.

do not support the sharp (~ 4 fold) drop in eQq 545
from $v' = 0-1$ reported by German [33]. For fur- 546
ther analysis, it is highly desirable to have ab initio 547
predictions of the trend in hyperfine parameters 548
for $v' > 1$. 549

5. Conclusions 550

We have examined the energy dependence of 551
the Zeeman parameters in the $\tilde{A}^2\Sigma^+$ state of OH 552
and OD, and the nuclear hyperfine parameters for 553
OD, using the technique of quantum beat spec- 554
troscopy. We find that the sign and magnitude of 555
the anisotropic g -factor g_1 for $v' = 0$ is consistent 556
with that expected from Curl's relationship, but at 557
higher energies this factor appears to change sign. 558
The rotational g -factor g_r is not well determined 559
and its energy dependence is not well character- 560
ized; however, its magnitude is consistent with 561
previous results and theoretical expectations. We 562
examined several explanations for the observed 563
energy dependence of g_1 , and conclude that the 564
most likely involves interaction of $\tilde{A}^2\Sigma^+$ with the 565
higher lying $^4\Pi$ state, which is known to lead to 566
predissociation at higher energies. We also deter- 567
mined the magnetic and electric quadrupole hy- 568
perfine constants for OD($\tilde{A}^2\Sigma^+$, $v' = 0-3$), the 569
constants for $v' = 2, 3$ being reported here for the 570

571 first time, and the derived values are consistent
572 with previous experimental results and available
573 ab initio calculations.

574 Acknowledgements

575 The authors gratefully acknowledge useful dis-
576 cussions with J.M. Brown and R.N. Zare. This
577 work was supported by the National Science
578 Foundation under Grant CHE-9702803.

579 References

- 580 [1] G. Herzberg, *Molecular Spectra and Molecular Structure*
581 *I. Spectra of Diatomic Molecules*, Van Nostrand, Prince-
582 *ton*, 1950.
- 583 [2] G. Herzberg, *The Spectra and Structures of Simple Free*
584 *Radicals*, Cornell University Press, Ithaca, 1971.
- 585 [3] A.G. Gaydon, H.G. Wolfhard, *Proc. R. Soc. A* 208 (1951)
586 63.
- 587 [4] H.P. Broida, W.R. Kane, *Phys. Rev.* 89 (1953) 1053.
- 588 [5] G.C. Dousmanis, T.M. Sanders Jr., C.H. Townes, *Phys.*
589 *Rev.* 100 (1955) 1735.
- 590 [6] G. Ehrenstein, C.H. Townes, M.J. Stevenson, *Phys. Rev.*
591 *Lett.* 3 (1959) 40.
- 592 [7] H.E. Radford, *Phys. Rev.* 122 (1961) 114.
- 593 [8] H.E. Radford, *Phys. Rev.* 126 (1962) 1035.
- 594 [9] G.H. Dieke, H.M. Crosswhite, *J. Quant. Spectrosc.*
595 *Radiat. Transfer* 2 (1963) 97.
- 596 [10] H.E. Radford, *Phys. Rev. Lett.* 13 (1964) 534.
- 597 [11] R.L. Poynter, R.A. Beaudet, *Phys. Rev. Lett.* 21 (1968)
598 305.
- 599 [12] H.B. Palmer, D.W. Naegeli, *J. Mol. Spectrosc.* 28 (1968)
600 417.
- 601 [13] P. Felenbok, *Ann. Astrophys.* 26 (1963) 393.
- 602 [14] C. Carlone, F.W. Dalby, *Can. J. Phys.* 47 (1969) 1945.
- 603 [15] A. Marshall, R.L. deZafra, H. Metcalf, *Phys. Rev. Lett.* 22
604 (1969) 445.
- 605 [16] K.R. German, R.N. Zare, *Bull. Am. Phys. Soc.* 15 (1970)
606 82.
- 607 [17] K.M. Evenson, J.S. Wells, H.R. Radford, *Phys. Rev. Lett.*
608 25 (1970) 199.
- 609 [18] A. Carrington, N.J.D. Lucas, *Proc. R. Soc. A* 314 (1969)
610 567.
- 611 [19] A. Churg, D.H. Levy, *Astrophys. J.* 162 (1970) L161.
- 612 [20] P.M. Clough, A.H. Curran, B.A. Thrush, *Proc. R. Soc. A*
613 323 (1971) 541.
- 614 [21] K.P. Lee, W.G. Tam, R. Larouche, G.A. Woonton, *Can. J.*
615 *Phys.* 49 (1971) 2207.
- 616 [22] R.L. deZafra, A. Marshall, H. Metcalf, *Phys. Rev. A* 3
617 (1971) 1557.
- 618 [23] E.A. Scarl, F.W. Dalby, *Can. J. Phys.* 49 (1971) 2825.
- [24] B.G. Elmergreen, W.H. Smith, *Astrophys. J.* 178 (1972) 619
557. 620
- [25] K.R. German, T.H. Bergeman, E.M. Weinstock, R.N. 621
Zare, *J. Chem. Phys.* 58 (1973) 4304. 622
- [26] E.M. Weinstock, R.N. Zare, *J. Chem. Phys.* 58 (1973) 623
4319. 624
- [27] M.A.A. Clyne, J.A. Coxon, A.R. Woon Fat, *J. Mol.* 625
Spectrosc. 46 (1973) 146. 626
- [28] J.H. Brophy, J.A. Silver, J.L. Kinsey, *Chem. Phys. Lett.* 28 627
(1974) 418. 628
- [29] K.R. German, *J. Chem. Phys.* 63 (1975) 5252. 629
- [30] J.A. Coxon, *J. Mol. Spectrosc.* 58 (1975) 1. 630
- [31] J.A. Coxon, R.E. Hammersley, *J. Mol. Spectrosc.* 58 631
(1975) 29. 632
- [32] D. Wilcox, R. Anderson, J. Peacher, *J. Opt. Soc. Am.* 65 633
(1975) 1368. 634
- [33] K.R. German, *J. Chem. Phys.* 64 (1976) 4192. 635
- [34] D.K. Killinger, C.C. Wang, M. Hanabusa, *Phys. Rev. A* 13 636
(1976) 2145. 637
- [35] J.L. Destombes, C. Marliere, F. Rohart, *J. Mol. Spectrosc.* 638
67 (1977) 93. 639
- [36] J.M. Brown, M. Kaise, C.M.L. Kerr, D.J. Milton, *Mol.* 640
Phys. 36 (1978) 553. 641
- [37] J. Brzozowski, P. Erman, M. Lyyra, *Phys. Scr.* 17 (1978) 642
507. 643
- [38] P. Lebow, F. Raab, H. Metcalf, *Phys. Rev. Lett.* 42 (1979) 85. 644
- [39] J.J. ter Meulen, G.W.M. van Mierlo, A. Dymanus, *Phys.* 645
Rev. Lett. 43 (1979) 29. 646
- [40] F. Raab, T. Bergeman, D. Lieberman, H. Metcalf, *Opt.* 647
Lett. 5 (1980) 427. 648
- [41] T. Bergeman, P. Erman, Z. Haratym, M. Larsson, *Phys.* 649
Scr. 23 (1981) 45. 650
- [42] F. Raab, T. Bergeman, D. Lieberman, H. Metcalf, *Phys.* 651
Rev. A 24 (1981) 3120. 652
- [43] J.A. Coxon, S.C. Foster, *J. Mol. Spectrosc.* 91 (1982) 243. 653
- [44] J.J. ter Meulen, W.A. Majewski, W.L. Meerts, A. Dym- 654
anus, *Chem. Phys. Lett.* 94 (1983) 25. 655
- [45] K.I. Peterson, G.T. Fraser, W. Klemperer, *Can. J. Phys.* 62 656
(1984) 1502. 657
- [46] P. Andresen, A. Bath, W. Groger, H.W. Luelf, G. Meijer, 658
J.J. ter Meulen, *Appl. Opt.* 27 (1988) 365. 659
- [47] D.D. Nelson Jr., A. Schifman, D.J. Nesbitt, D.J. Yaron, *J.* 660
Chem. Phys. 90 (1989) 5443. 661
- [48] A. Arnold, W. Ketterle, J. Wolfrum, *Appl. Phys. B* 51 662
(1990) 99. 663
- [49] T. Dreier, D.J. Rakestraw, *Appl. Phys. B* 50 (1990) 475. 664
- [50] J.A. Gray, R.L. Farrow, *J. Chem. Phys.* 95 (1991) 7054. 665
- [51] K.P. Huber, F. Holland, J.A. Coxon, *J. Chem. Phys.* 96 666
(1992) 1005. 667
- [52] D.E. Heard, D.R. Crosley, J.B. Jeffries, G.P. Smith, A. 668
Hirano, *J. Chem. Phys.* 96 (1992) 4366. 669
- [53] I.M. Povey, R.T. Carter, H. Bitto, J.R. Huber, *Chem.* 670
Phys. Lett. 248 (1996) 470. 671
- [54] R.T. Carter, I.M. Povey, H. Bitto, J.R. Huber, *J. Chem.* 672
Phys. 104 (1996) 5365. 673
- [55] J.J.L. Spaanjaars, J.J. ter Meulen, G. Meijer, *J. Chem.* 674
Phys. 107 (1997) 2242. 675

- 676 [56] A.A. Suvernev, R. Tadday, T. Drier, *Phys. Rev. A* 58 (1998) 4102. 708
677 (1998) 4102. 709
678 [57] J. Czarny, P. Felenbok, H. Lefebvre-Brion, *J. Phys. B* 4 (1971) 124. 710
679 (1971) 124. 711
680 [58] A.G. Gaydon, I. Kopp, *J. Phys. B* 4 (1971) 752. 712
681 [59] S. Green, *J. Chem. Phys.* 58 (1973) 4327. 713
682 [60] M.L. Sink, A.D. Bandrauk, *Chem. Phys. Lett.* 65 (1979) 246. 714
683 (1979) 246. 715
684 [61] E.F. van Dishoeck, A. Dalgarno, *J. Chem. Phys.* 79 (1983) 873. 716
685 (1983) 873. 717
686 [62] S.R. Langhoff, H. Partridge, *J. Mol. Spectrosc.* 105 (1984) 261. 718
687 (1984) 261. 719
688 [63] E.F. van Dishoeck, M.C. van Hemert, A.C. Allison, A. Dalgarno, *J. Chem. Phys.* 81 (1984) 5709. 720
689 (1984) 5709. 721
690 [64] S.J. Singer, K.F. Freed, Y.B. Band, *Adv. Chem. Phys.* 61 (1985) 1. 722
691 (1985) 1. 723
692 [65] S. Lee, C.J. Williams, K.F. Freed, *Chem. Phys. Lett.* 130 (1986) 271. 724
693 (1986) 271. 725
694 [66] S. Lee, K.F. Freed, *J. Chem. Phys.* 87 (1987) 5772. 726
695 (1987) 5772. 727
696 [67] D.R. Yarkony, *J. Chem. Phys.* 97 (1992) 1838. 728
697 (1992) 1838. 729
698 [68] S. Lee, *Chem. Phys. Lett.* 240 (1995) 595. 730
699 (1995) 595. 731
700 [69] S. Lee, *Chem. Phys. Lett.* 243 (1995) 250. 732
701 (1995) 250. 733
702 [70] S. Lee, *J. Phys. Chem.* 99 (1995) 13380. 734
703 (1995) 13380. 735
704 [71] S. Lee, *J. Chem. Phys.* 103 (1995) 3501. 736
705 (1995) 3501. 737
706 [72] S. Lee, *J. Chem. Phys.* 104 (1996) 1912. 738
707 (1996) 1912. 739
[73] G. Parlant, D.R. Yarkony, *J. Chem. Phys.* 110 (1999) 363. 740
[74] M.P. de Lara Castells, A. Mitrushenkov, P. Palmieri, F. le Quèrè, C. Leonard, P. Rosmus, *Mol. Phys.* 98 (2000) 1713. 741
[75] M. Glass-Maujean, J. Breton, P.M. Guyon, *Chem. Phys. Lett.* 63 (1979) 591. 742
[76] J.T. Brandon, S.A. Reid, D.C. Robie, H. Reisler, *J. Chem. Phys.* 97 (1992) 5246. 743
[77] S.A. Reid, J.T. Brandon, H. Reisler, *J. Phys. Chem.* 97 (1993) 540. 744
[78] B. Kim, K. Yoshihara, *J. Chem. Phys.* 99 (1993) 1433. 745
[79] B. Kim, K. Yoshihara, S. Lee, *Phys. Rev. Lett.* 73 (1994) 424. 746
[80] B.R. Lewis, S.S. Banerjee, S.T. Gibson, *J. Chem. Phys.* 102 (1995) 6631. 747
[81] R.F. Curl, *Mol. Phys.* 5 (1965) 585. 748
[82] Y. Tang, J.P. Schmidt, S.A. Reid, *J. Chem. Phys.* 110 (1999) 5734. 749
[83] Ju Xin, S.A. Reid, *J. Chem. Phys.* 112 (2000) 10067. 750
[84] J. Xin, S.A. Reid, F. Santoro, C. Petrongolo, *J. Chem. Phys.* 115 (2001) 8868. 751
[85] J. Xin, S.A. Reid, *J. Chem. Phys.* 116 (2002) 515. 752
[86] R.T. Carter, J.R. Huber, *Chem. Soc. Rev.* 29 (2000) 305. 753
[87] J. Xin, H. Fan, I. Ionescu, D. Kuffel, S.A. Reid, *J. Mol. Spectrosc.*, in press. 754
[88] H.E. Radford, *Phys. Rev. A* 136 (1964) 1571. 755
[89] A. Carrington, D.H. Levy, T.A. Miller, *Adv. Chem. Phys.* 18 (1970) 149. 756
[90] I.C. Bowater, J.M. Brown, A. Carrington, *Proc. R. Soc. London, Ser. A* 333 (1973) 265. 757
[91] L. Veseth, *J. Mol. Spectrosc.* 63 (1976) 180. 758
[92] H. Christensen, L. Veseth, *J. Mol. Spectrosc.* 72 (1978) 438. 759
[93] H. Lefebvre-Brion, R.W. Field, *Perturbations in the spectra of diatomic molecules*, Academic Press, Orlando, 1986. 760
[94] J.M. Brown, K. Dumper, C.R. Parent, *Mol. Phys.* 36 (1978) 1149. 761
[95] J.E. Nafe, E.B. Nelson, *Phys. Rev.* 73 (1948) 718. 762
[96] E. Hirota, *High-resolution Spectroscopy of Transient Molecules*, Springer, Berlin, 1985. 763